A Moving Liver Phantom in An Anthropomorphic Thorax for SPECT MP Imaging

Sotiris Panagi (st009570@stud.fit.ac.cy)
Frederick Research Center & Frederick University https://orcid.org/0000-0001-5033-5907
Anastasia Hadjiconstanti
Frederick Research Center
George Charitou
Frederick Research Center
Demetris Kaolis
Nicosia General Hospital: Geniko Nosokemeio Leukosias
Ioannis Petrou
Nicosia General Hospital: Geniko Nosokemeio Leukosias
Costas Kyriacou
Frederick University
Yiannis Parpottas
Frederick Research Center & Frederick University

Research Article

Keywords: liver phantom, SPECT/CT MPI, cranio-caudal respiratory motion, MP artifacts, liver activity, supine and prone imaging

Posted Date: June 23rd, 2021

DOI: https://doi.org/10.21203/rs.3.rs-638257/v1

Version of Record: A version of this preprint was published at Physical and Engineering Sciences in Medicine on January 1st, 2022. See the published version at https://doi.org/10.1007/s13246-021-01081-4.

Abstract

Cranio-caudal respiratory motion and liver activity cause a variety of complex myocardial perfusion (MP) artifacts, especially in the inferior myocardial wall, that may also mask cardiac defects. To assess and characterize such artifacts, an anthropomorphic thorax with moving thoracic phantoms can be utilized in SPECT MP imaging. In this study, a liver phantom was developed, and anatomically added into an anthropomorphic phantom, that encloses an ECG beating cardiac phantom and breathing lungs phantom. A cranio-caudal respiratory motion was also developed for the liver phantom and it was synchronized with the corresponding ones of the cardiac and lungs phantoms. This continuous motion could also be further divided into dynamic respiratory phases, from end-exhalation to end-inspiration, to perform SPECT acquisitions in different respiratory phases. The motion parameters, displacements and volumes, were validated by the acquired CT slices, the OsiriX and Vitrea software. Sample SPECT/16-slice-CT myocardial MP acquisitions were also performed and compared to the literature. The cardiac, lungs and liver phantoms can precisely perform, in time interval of 0.1 sec, physiological thoracic motions within an anthropomorphic thorax. This dynamic phantom assembly can be utilized for SPECT MP supine and, for first time, prone imaging to access and characterize artifacts due to different cranio-caudal respiratory amplitudes and cardiac-liver activity ratios.

Introduction

Myocardial perfusion imaging (MPI) is subjected to a variety of artifacts that can limit the performance of the study. Artifacts can arise at any stage in the MP process, and they can be grouped into issues related to the patient, equipment, or technologist [1].

Patient-related artifacts in MPI, not originated from the heart, are mainly due to attenuation, thoracic motions, and sub-diaphragmatic activity. Attenuation artifacts are caused due to the anatomy surrounding the heart [2]. Motion artifacts cause blurring along the motion direction, and they are mainly due to the cranio-caudal respiratory motion of the heart [3]. Sub-diaphragmatic organs adjacent to the heart, mainly the liver, present prominent radioactivity which mainly interferes with the adjacent inferior wall of the left ventricle due to photon scattering [4]. The radioactivity of the moving heart and liver, during the cranio-caudal respiratory motion, overlap and as a result it artificially decreases or increases the uptake in the adjacent regions of the heart. [5]. Different amplitudes of these motions may result in different spillover of the liver activity into the adjacent heart walls. The liver (a) activity, (b) proximity to the heart, and (c) motion amplitude during respiration are the main contributing parameters to MP artifacts due to liver [5]. This varying liver interaction causes a complex and clinically unpredictable variation in MPI which may mask cardiac defects in the case of an uptake increase, or cause artifactual defects in the case of an uptake decrease, or may create a complex combination of these two cases.

Phantoms that closely simulate tissues, anatomy and motion are important to investigate these artifacts and optimize the MP imaging technique, without exposing patients to radiation [6,7]. To investigate this varying liver interaction and its impact on defect detection, phantoms should be able to simulate various

(a) cardiac-liver activity (CLA) ratios, (b) cardiac-liver proximities (CLP) and (c) oscillation amplitudes during respiration.

In single-photon emission computed tomography (SPECT) MPI, the Tc99m extra-cardiac activity (ECA) due to liver was studied using static and manually moving torso phantoms with static cardiac and liver compartments [4,5,8,9]. Germano et al. [4] investigated ECA, using a static torso phantom with an enclosed custom-made lucite wedged-shaped liver compartment for three different values of CLA. Nuyts et al. [8], using a static perspex cylinder with an enclosed plastic water-bag liver compartment, studied MP artifacts due to ECA for a CLA value. Heller et al. [9], using an almost similar phantom as Nuyts et al. [8], also studied MP artifacts due to ECA for a higher CLA value. Pitman et al. [5], using an acrylic cylinder with an enclosed static saline-bag liver compartment, examined the effects of ECA interaction for two different CLA values and two different diaphragmatic motion amplitudes by manually moving the cylinder during SPECT MP acquisitions.

In our previous studies [2,3,10–12], we acquired SPECT/CT images using an anthropomorphic thorax which enclosed moving thoracic compartments: (a) a cardiac phantom of an ECG beating and moving left ventricle during respiration in the cranio-caudal direction, and (b) a breathing phantom of a pair of lungs. These motions could be controlled in time interval of 0.1 sec and various parameters of the motions can vary such as the ejection fraction, heart rate, breath rate and tidal volume. In these studies, we characterized MP artifacts, evaluate physicians reports on cardiac defects, and correct the images for motion.

In this paper, we present the development of a liver phantom with motion, implemented within an anthropomorphic thorax and synchronized with the existing thoracic motions, and the evaluation of the phantom assembly in investigating MP artifacts due to liver.

Materials And Methods

Liver Phantom

A liver phantom was designed taking into consideration the liver density, shape and size, as well as its position within the thorax and proximity to the heart. For this purpose, the MeshMixer [13] and 3D Slicer [14] design softwares were used. In order to be able to simulate various cardiac-liver activity ratios during SPECT/CT acquisitions, the liver phantom was designed as a hollow cavity with a wall thickness of 2 mm. Two holes were added to the design to fill the phantom with water and radiopharmaceutical, with diameters of 20 mm and 4 mm, respectively. A diagonal base was also added to the design, at the outer inferior border of the liver, to be able to tighten a rod in order to hold the liver in position within the thorax.

The liver phantom was 3D-printed with a transparent resin material with a density of 1.06 g/cm^3. Solid-water caps were manufactured to seal the abovementioned holes. The female-thread and the rod were also manufactured from a solid-water material (Fig. 1).

Motion Mechanism

A mechanism, controlled by a programmable logic controller (PLC), was manufactured to provide motion to the liver phantom. The motion is transferred via the rod which at one end, in the thorax, is attached to the phantom and at the other end, outside the thorax, is attached to the mechanism. The rod enters the thorax via a water-tight hole at the base of the thorax. The mechanism is aligned with the rod, and it is attached at the outer base of the thorax phantom (Fig. 2). The main components of the mechanism to generate and validate the liver motion are: (a) the motor, (b) the screwed-rod system, (c) the laser distance sensor with its reflector and (d) the two proximity sensors.

Figure 3 shows the main parts of the mechanism. The PLC drives the motor and, consequently, oscillates the screwed-rod system (outwards-inwards), which is attached to the front of the motor. The moving screwed-rod system also moves an aluminium structure on which (a) the reflector of the laser distance sensor and (b) the rod of the liver phantom, are attached, as showed in Fig. 3. The laser sensor is connected directly to the PLC and its screen-monitor provides feedback about the motion, in the millimetre scale. Note that the laser distance sensor does not move, while its reflector moves together with the moving aluminium structure. The two proximity sensors are positioned on the mechanism, without moving, vertical to the motion of the screwed-rod, 3 cm apart from each other, as seen in the figure. They define the minimum and maximum limits of the motion amplitude, and they stop the motion in the rare event that the reflector pass these limits.

The cardiac-liver proximity is defined by the length of the liver rod that enters in the thorax. This proximity can be set between 0.5 and 2.5 cm, in distance intervals of 0.5 cm. For this purpose, the rod can be properly tightened on the mechanism using the corresponding drawn marks on the rod. For prone imaging, this mechanism together with the rest of the phantom assembly (Fig. 2) is turned by 180°.

Liver motion

A VisiLogic ladder program was developed in the PLC to describe the cranio-caudal motion of the liver during respiration, and consequently to control the motion of the motor.

The equation of motion is as follows:

$$X_L(t) = X_o sin(at + 90°) \qquad (1)$$

where $X_L(t)$ is the position (in mm) of the phantom with respect to time, X_o is the maximum amplitude of the oscillation, t is the counting time in intervals of 0.1 sec, $a = \frac{2\pi}{T}$, and T is the time-period of the motion.

Note that the same equation is utilized for the cranio-caudal cardiac motion during respiration [12]. The counting time and time-period of the liver and cardiac motions are synchronized with the equation for breathing. At *t = 0 sec*, the lungs phantom is at end-exhalation and the cardiac-liver phantoms are in the corresponding anatomical positions (cranio/upper position = 0 mm). At one time-period, defined by the

breath rate, the cardiac-liver phantoms, following Eq. 1, have been oscillated, together with the inferior portion of the lungs phantom at the level of the diaphragm, to the caudal/lower position, while the lungs, following the breathing equation [12], are at end-inhalation. For a specific breath rate, all phantoms can perform normal or deep respiratory motion. The lower caudal/upper position is 15 or 27 mm for the normal or deep respiratory motion, respectively, while the air tidal volume in the lungs is 450 or 550 mL for the normal or deep respiratory motion, respectively.

In addition to the abovementioned synchronized PLC mode of the continuous motion, a synchronized PLC mode of dynamic respiratory phases was also developed. The respiratory motion was divided into four static phases from end-exhalation to end-inhalation. The displacement of the cardiac-liver phantoms from the initial position and the air-volume of the lungs phantom at each static phase, for normal and deep respiration, are shown in Table 1. A motion, in the dynamic respiratory phase mode, is performed between two successive static phases. In this mode, the phantoms follow the same equations. As seen in Table 1, for each respiration, normal or deep, three different such motions can be performed.

During motion or at any static phase, the mechanical accuracy of the cranio-caudal displacement with respect to time can be seen on the laser distance sensor (± 1 mm) while the accuracy of the lungs volume with respect to time was measured by using a custom-made structure. In particular, the lungs were immersed in a tank which was totally filled with water. Air could be provided to the lungs by its mechanical system, via two water-tight openings located on the top side of the tank. Consequently, the water was raised in a graduated cylinder (± 5 mL) which was attached on the top side of the tank.

Table 1
The motion parameters of the dynamic respiratory phases mode: lungs' volume and cardiac-liver displacement.

	Normal Respiration Deep Respiration				
Dynamic respiratory phase	**Oscillation between static phases**	**Lungs' volume (mL)**	**Cardiac-liver displacement (mm)**	**Lungs' volume (mL)**	**Cardiac-liver displacement (mm)**
1	1↔2	1100↔1145	0↔5	1100↔1155	0↔5
2	2↔3	1145↔1344	5↔10	1155↔1398	5↔20
3	3↔4	1344↔1550	10↔15	1398↔1650	20↔27

SPECT/CT and CT acquisitions

The Toshiba Aquilion RXL 16-CT system of the Limassol General Hospital was utilized to perform CT acquisitions of the phantom assembly. The slice thickness was 0.5 mm (1200 slices per image), the tube voltage was set at 120 kV_p and the current at 100 mA. The OsiriX [15] and Vitrea [16] softwares were used

to measure (a) the liver volume, (b) the different cardiac-liver displacements and lungs volume in each respiratory phase, and (c) the different cardiac-liver proximities.

Also, the GE Discovery-670-DR SPECT/16-slice-CT of the Nicosia General Hospital was utilized to perform acquisitions of the phantom assembly, in supine and prone position, for different motion settings. The acquisitions were performed using a routine clinical protocol with two Low-Energy High-Resolution collimators in 90° (L-mode) orientation. Data were acquired in 60 projections, 20 seconds per projection, over 180° of rotation, with a matrix of 64x64. An activity of 15 MBq of Tc99m was injected into the myocardium wall of the left ventricle, based on an estimate of 1.2% uptake of a clinically relevant administered activity [17]. A 20% energy window was centered over the 140 keV photopeak of Tc99m. CT images were acquired around the heart region, with 5 mm slice thickness and a matrix of 512x512. SPECT data were reconstructed using the ordered subset expectation maximization algorithm with 2 iterations and 10 subsets. A Butterworth filter (cut-off: 0.52, power: 5) was applied on the reconstructed images. SPECT data were also scattered and attenuated corrected.

Results

Figure 4 shows the coronal, sagittal and axial CT slices as well as the 3D view of the thorax with its enclosed thoracic phantoms, in supine and in prone positions. The images were acquired by the abovementioned CT system and processed with the Vitrea software. The position of the newly added liver phantom within the thorax is presented with yellow colour. The liver volume was measured to be 1150 mL.

Figure 5 shows a zoomed region of coronal CT slices of the phantom assembly when the cardiac phantom was at systole (left) and at diastole (right). The cardiac-liver proximity was mechanically set to be 0.5 cm, when the cardiac phantom was at diastole. It was measured by the OsiriX software to be 0.51 cm, and consequently, the corresponding distance, when the cardiac phantom was at systole, was measured to be 1.53 cm, since the beating cardiac phantom contracts by about 1 cm. The same measurements were repeated for all different, mechanically possible, cardiac-liver proximities, from 0.5 to 2.5 cm when the cardiac phantom was at diastole.

Figure 6 shows coronal (top row), sagittal (middle row) and axial (bottom row) slices of the phantom assembly at the four static phases in deep breathing: phase-1 (1st column), phase-2 (2nd column), phase-3 (3rd column) and phase-4 (4th column). The cranio-caudal displacement is indicated with the red lines. The cardiac-liver proximity was set to 0.5 cm and the cardiac phantom at systole. The volume of the lungs and the downward displacement were measured with the OsiriX software, and they were in agreement with the values of Table 1.

Figure 7 shows the SPECT/CT 5-segments polar maps of the phantom assembly with the following settings: an ECG beating left ventricle, without cardiac defects, a CLA activity ratio of 1:0.5, in supine position and CLP of 0.5 cm (a and b), in prone position and CLP of 2 cm (c and d), in deep (b) and normal (d) respiratory motion. Note that, the value of the CLP is given for the cardiac phantom at diastole.

Prone imaging was performed with a CLP of 2 cm instead of 0.5 cm, as set in supine imaging, since in prone position the inferior myocardial wall and the diaphragm are well separated [18]. Also, prone imaging was performed for normal and supine imaging for deep respiratory motion, respectively, since prone position reduce the degree of patient motion [19]. The polar maps were visually evaluated by a nuclear medicine physician and they are discussed in the next section.

Discussion

A liver phantom was designed, manufactured, and anatomically added in the antihomophobic thorax, as described above. A continuous liver motion, during cranio-caudal respiratory motion, was developed and synchronized with the motions of the other existing thoracic phantoms. In addition, synchronized motions in respiratory phases (dynamic respiratory phase mode) from end-exhalation to end-inhalation were developed for all the thoracic phantoms. During the cranio-caudal respiratory motion, the displacement of the phantoms and the volume of the lungs' phantom were accurately measured, mechanically, with a laser distance sensor and a graduated cylinder, respectively. These motion parameters were also measured and validated from the acquired CT slices, the OsiriX and Vitrea software.

Further, SPECT/CT acquisitions were performed using the phantom assembly in supine and prone positions. A nuclear medicine physician visually evaluated the reconstructed polar maps. As in previous phantom and patient studies [2,18,19], motion artifacts were induced in the anterior and inferior myocardial walls. However, in prone imaging, the diaphragmatic attenuation in the inferior wall was reduced [18,19].

Previously, only one SPECT/^{153}Gd phantom study [5] was performed, in supine position, using a manually moving torso phantom, which enclosed static compartments, to access MP artifacts due to different respiratory motions and cardiac-liver activity ratios. This anthropomorphic thorax, with precisely controlled physiological thoracic motions, simulates a more realistic scenario. For the first time, a phantom assembly with motions can be imaged not only in supine but also in prone position.

Conclusions

In this paper, we have presented the development and evaluation of a liver moving phantom, which was implemented with an anthropomorphic thorax. The thoracic phantoms of the ECG beating left ventricle, the inflatable lungs and the liver can perform a synchronized cranio-caudal respiratory motion within an anthropomorphic thorax. This oscillatory motion is controlled by a PLC in time interval of 0.1 sec. This motion can be continuous or in phases, for normal or deep respiration. Several motion limitations of other phantoms have been overcome.

SPECT/CT MP acquisitions can be performed using this phantom assembly, in supine and prone position, with/out different sizes of cardiac defects, for different cardiac-liver activity ratios, cardiac-liver

proximities and respiratory amplitudes. Thus, using this phantom assembly, various types of MP artifacts can be accessed and characterized, and their impact on defect detection can be investigated, in detail.

Declarations

Conflict of interest

Authors declare that they have no conflict of interest.

Acknowledgements

We gratefully acknowledge the staff of the Radiological Department of the Limassol General Hospital and the staff of the Department of Nuclear Medicine of the Nicosia General Hospital for helping in the acquisitions. This study was co-funded by the European Regional Development Fund and the Republic of Cyprus through the Research and Innovation Foundation (Project EXCELLENCE/1216/0085).

References

1. Burrell S and MacDonald A (2006) Artifacts and Pitfalls in Myocardial Perfusion Imaging. J Nucl Med Technol 34:193:211
2. Chrysanthou-Baustert I, Polycarpou I, Demetriadou O, Livieratos L, Lontos A, Parpottas Y et al (2017) Characterization of attenuation and respiratory motion artifacts and their influence on SPECT MP Image evaluation using a dynamic phantom assembly with variable cardiac defects. J Nucl Cardiol 24(2), 698-707
3. Polycarpou I, Chrysanthou-Baustert I, Demetriadou O, Parpottas Y, Marsden PK, Livieratos L et al (2015) Impact of respiratory motion correction on SPECT myocardial perfusion imaging using a mechanically moving phantom assembly with variable cardiac defects, J Nucl Cardiol 22(6). https://doi.org/10.1007/s12350-015-0323-0
4. Germano G, Chua T, Kiat H, Areeda SJ and Berman D (1994) A Quantitative Phantom Analysis of Artifacts Due to Hepatic Activity in Technetium-99m Myocardial Perfusion SPECT Studies. J Nucl Med 35(2):356-9
5. Pitman A, Kalff V, Van Every B, Risa B, Barnden L, Kelly M (2005) Contributions of subdiaphragmatic activity, attenuation, and diaphragmatic motion to inferior wall artifact in attenuation-corrected Tc99m myocardial perfusion SPECT. J Nucl Cardiol 12:401-409
6. Anon (1989) Tissue substitutes in radiation dosimetry and measurement. ICRU Report 44. Bethesda, United States
7. Anon (1992) Phantoms and computational models in therapy. ICRU Report 48. Bethesda, United States

8. Nuyts J, Dupont P, Van den Maegdenbergh V, Vleugels S, Suetens P, Mortelmans L (1995) A study of the liver-heart artifact in emission tomography. J Nucl Med 36(1):133-9
9. Heller EN, DeMan P, Liu Y-H, Dione DP, Zubal IG, Wackers FJTh, Sinusas AJ (1997) Extra-cardiac activity complicates quantitative cardiac SPECT imaging using a simultaneous transmission-emission approach. J Nucl Med 38:1882-1890
10. Chrysanthou-Baustert I, Parpottas Y, Demetriadou O, Christofides S, Yiannakkaras Ch, Kaolis D et al (2013) Diagnostic sensitivity of SPECT myocardial perfusion imaging using a pumping cardiac phantom with inserted variable defects. J Nucl Cardiol 20, 609-615
11. Lontos A, Antoniou A, Chrysanthou-Baustert I, Christofides S, Demetriadou O, Parpottas Y et al (2016) Construction of Inflatable Lungs to Simulate Respiratory Motion in Myocardial Perfusion Imaging, Springer. In: XIV Mediterranean Conference on Medical and Biological Engineering and Computing, pp. 1331-1335. Springer, Cyprus
12. Panagi S, Antoniou A, Chrysanthou-Baustert I, Kaolis D, Demetriadou O, Kyriacou C, Parpottas Y (2020) Controlled Thoracic Motions of an Anthropomorphic Phantom for Myocardial Perfusion Imaging, Springer Nature Switzerland. In: XV Mediterranean Conference on Medical and Biological Engineering and Computing, MEDICON 2019, IFMBE Proceedings 76, pp. 727–734
13. https://www.meshmixer.com. Accessed 28 April 2019
14. 3D Slicer Documentation. https://readthedocs.org/projects/slicer/downloads/pdf/latest/. Accessed 10 May 2019
15. OsiriX HD User Manual. http://pixmeo.pixmeo.com/documents/OsiriXUserManualExtract.pdf. Accessed 16 November 2020
16. Vital Images, Inc (2020) Vitrea View User Guide. https://eiview.ochsner.org/vitrea-view/help/en/userGuide/userGuide.pdf. Accessed 25 November 2020
17. Hesse B, Kristina-Tagil A, Cuocolo C, Anagnostopoulos M, Bardies J, Bax F et al (2005) EANM/ESC procedural guidelines for myocardial perfusion imaging in nuclear cardiology. Eur J Nucl Med Mol Imaging 32(7):855-97
18. Kiat H, Van Train KF, Friedman JD, Germano G, Silagan G, Wang FP, Maddahi J, Prigent F, Berman DS (1992) Quantitative stress-redistribution thallium-201 SPECT using prone imaging: methodologic development and validation. J Nucl Med 33(8):1509-15. PMID: 1634943
19. Segall GM, Davis MJ (1989) Prone versus supine thallium myocardial SPECT: a method to decrease artifactual inferior wall defects. J Nucl Med 30(4):548-55. PMID: 2661750

Figures

Figure 1

(Left) The 3d design of the liver phantom, and (right) the manufactured liver phantom with the (1) attached female-thread, (2) the caps, and (3) the rod. Two opposite views (left and right) are shown.

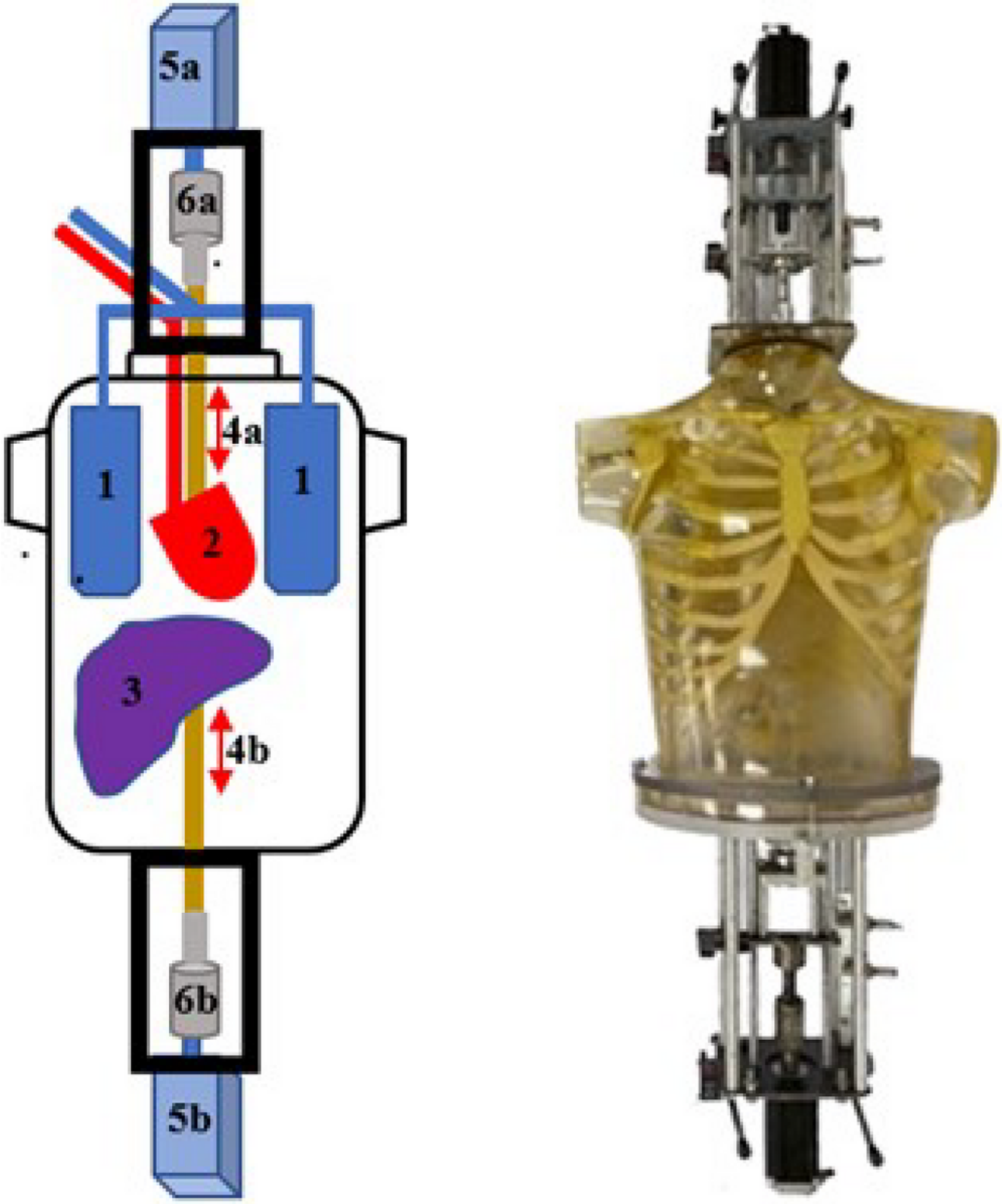

Figure 2

(Left) A schematic diagram of the anthropomorphic thorax, its enclosed (1) lungs, (2) cardiac, (3) liver phantoms, and its attached mechanisms to support the cranio-caudal respiratory motion of the cardiac (4-6a) and liver (4-6b) phantoms, where (4) are the phantom rods, (5) the motors, and (6) the screwed-rods. (Right) A photo of the anthropomorphic thorax with its enclosed thoracic phantoms and its attached mechanisms.

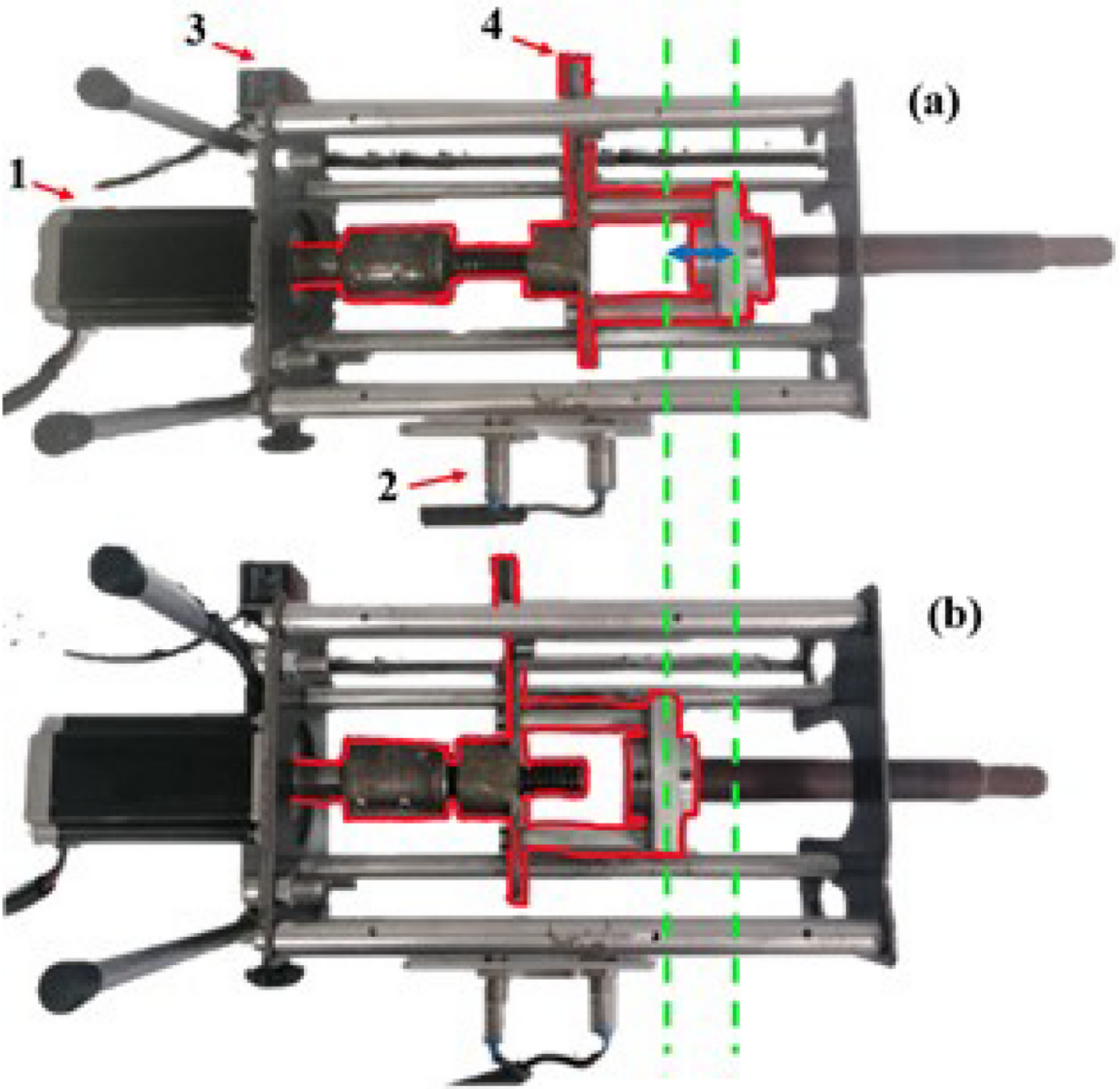

Figure 3

Top view of the cranio-caudal liver motion mechanism with (a) more and (b) less length of the liver rod into the thorax. The motor (1), the proximity sensors (2), the laser sensor (3) and its reflector (4) are shown. The screwed-rod is outlined with a red colour. The vertical green dotted lines help to visualize the motion.

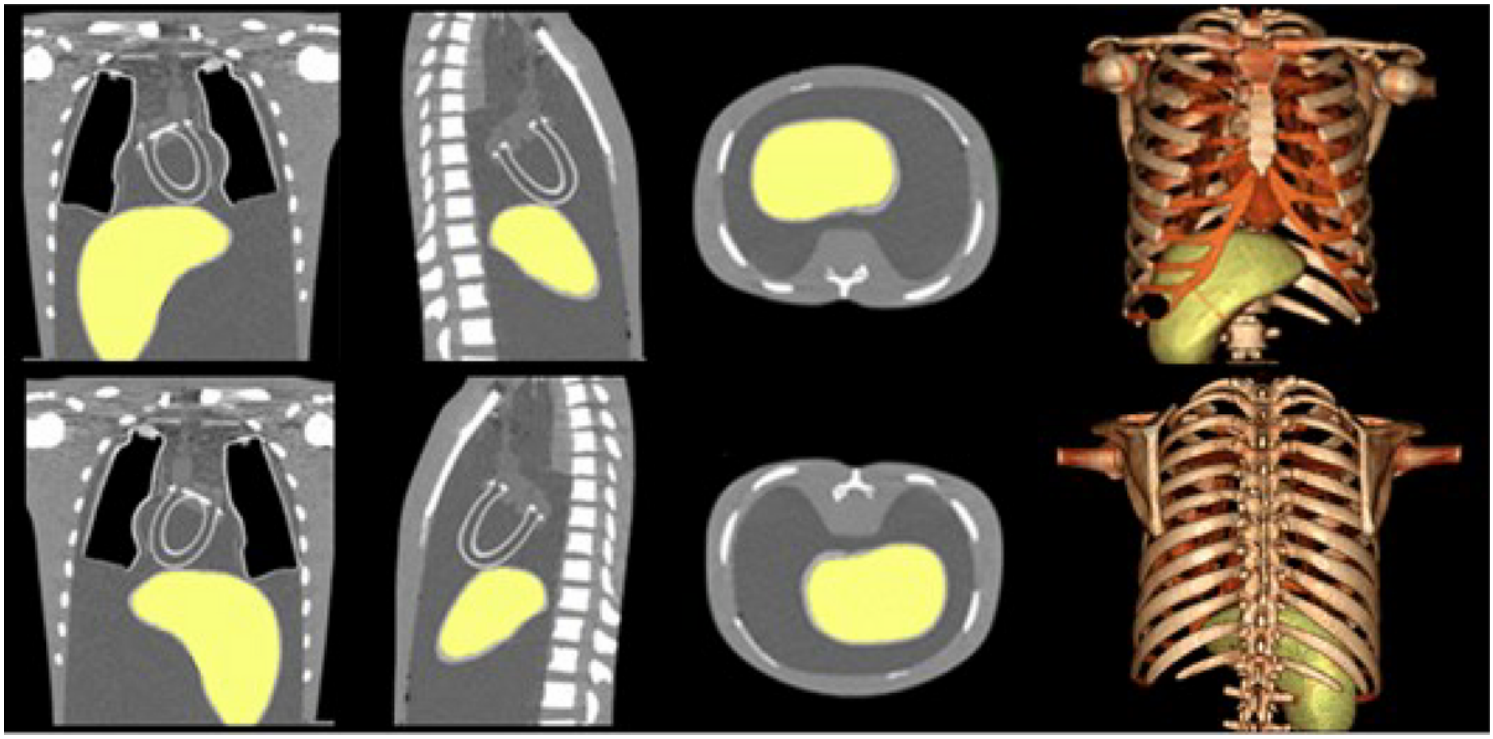

Figure 4

Coronal (1st column), sagittal (2nd column), axial (3rd column) slices, and a 3D view (4th column) of the phantom assembly in supine (top row) and prone (bottom row) positions. The images were acquired by the Toshiba Aquilion RXL 16-CT system and processed with the Vitrea software.

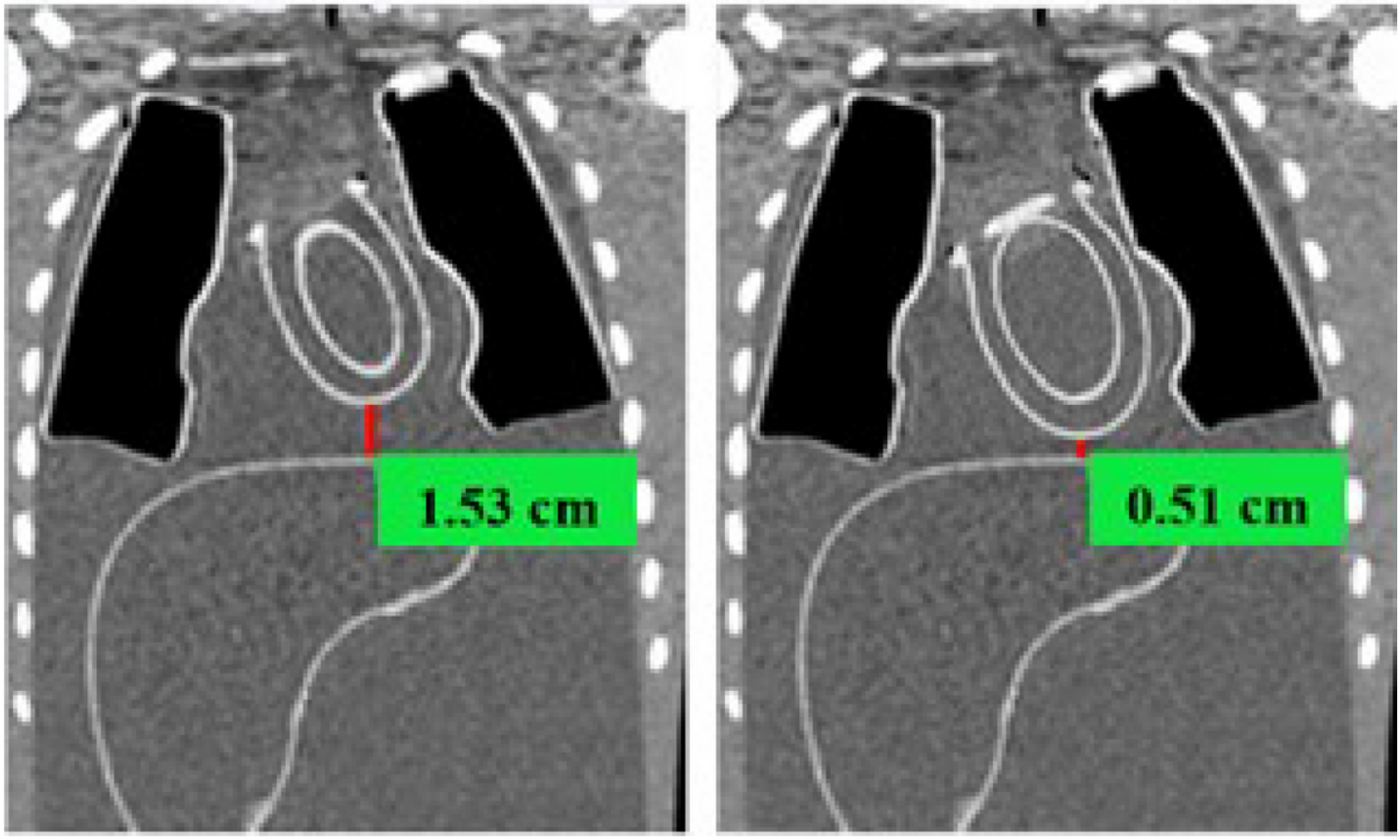

Figure 5

The cardiac-liver proximities, measured with the OsiriX software, when the cardiac phantom was at systole (left) and at diastole (right).

Figure 6

Coronal (top row), sagittal (middle row) and axial (axial row) slices of the phantom assembly at the four static phases in deep breathing: phase-1 (1st column), phase-2 (2nd column), phase-3 (3rd column) and phase-4 (4th column). The cardiac-liver proximity was set to 0.5 cm when the cardiac phantom was at diastole.

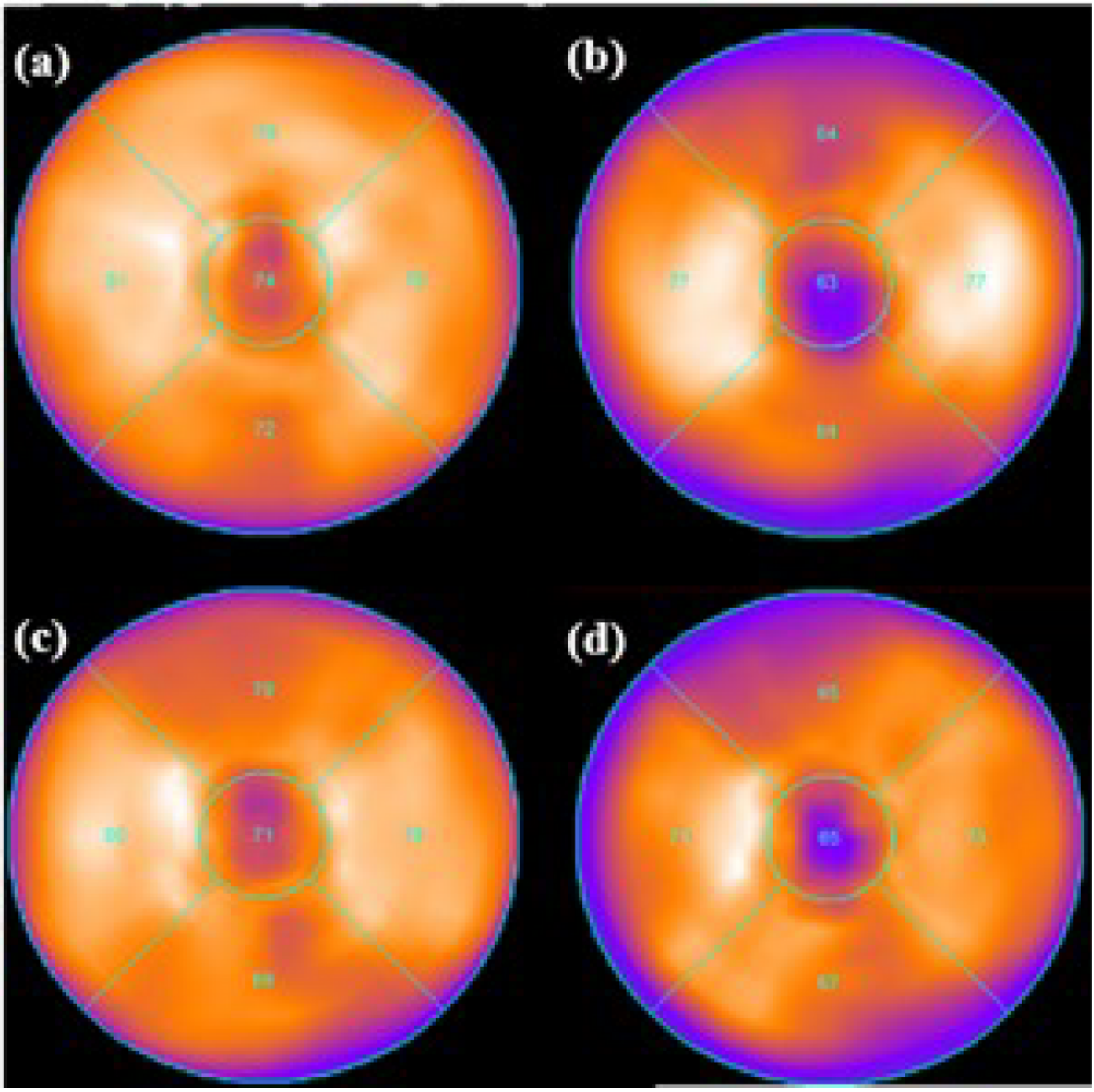

Figure 7

SPECT/CT 5-segments polar maps of the phantom assembly for the following settings: an ECG beating left ventricle, without cardiac defects, a CLA ratio of 1:0.5, in supine position and CLP of 0.5 cm (a and b), in prone position and CLP of 2 cm (c and d), in deep (b) and normal (d) respiratory motion.